Research Article | Vol. 24, No. 23 | 14 Nov 2016 | OPTICS EXPRESS 26956

Optics EXPRESS

Novel double step approach for optical sensing via microsphere WGM resonance

G. PALMA,[1] M. C. FALCONI,[1] F. STARECKI,[2] V. NAZABAL,[2] T. YANO,[3] T. KISHI,[3] T. KUMAGAI,[3] AND F. PRUDENZANO[1,*]

[1]*Department of Electrical and Information Engineering, Politecnico di Bari, Bari 70125, Italy*
[2]*Institute des Sciences Chimiques de Rennes, UMR 6226, Université de RENNES 1-CNRS, Rennes 35042 Cedex, France*
[3]*Department of Chemistry and Materials Science, Tokyo Institute of Technology, Tokyo 152-8550, Japan*
**francesco.prudenzano@poliba.it*
https://www.moe-group.it

Abstract: The use of resonant whispering gallery modes (WGMs) for sensing exhibits various drawbacks and critical points related to the microsphere and tapered optical fiber fabrication tolerance. The uncertainty on the fiber taper and microsphere geometry or the gap between the microsphere and the fiber taper can complicate or limit the actual use of these devices for sensing, requiring peculiar calibration of the WGM based sensing set-up. An alternative double-step approach is proposed in this paper. In particular, the geometrical parameters of the set-up are recovered preliminarily and then the rare earth parameters are recovered via simple transmittance/gain measurements. The method is based on a refined electromagnetic model of the device suitably integrated with a particle swarm optimization (PSO) approach. The percent errors made on the up-conversion coefficients C_{up} and C_3 are extremely low, being 0.75%, 0.05%, respectively. The procedure is very robust. It can be applied more in general, allowing the sensing of other physical parameters via simple transmittance measurements instead of wavelength shift ones, in both microsphere and microbubble based set-up.

OCIS codes: (140.4780) Optical resonators; (140.4480) Optical amplifiers; (060.2390) Fiber optics, infrared; (130.6010) Sensors; (130.3990) Micro-optical devices; (140.5680) Rare earth and transition metal solid-state lasers; (310.3840) Materials and process characterization; (160.2750) Glass and other amorphous materials; (140.3500) Lasers, erbium.

References and links

1. N. Miri and M. Mohammadzaheri, "Optical sensing using microspheres with different size and material," IEEE Sens. J. **14**(10), 3593–3598 (2014).
2. M. Charlebois, A. Paquet, L. S. Verret, K. Boissinot, M. Boissinot, M. G. Bergeron, and C. Nì Allen, "Differentiation between analyte absorption and homogenous index sensing in WGM biodetection," IEEE Sens. J. **13**(1), 229–233 (2013).
3. K. J. Vahala, "Optical microcavities," Nature **424**(6950), 839–846 (2003).
4. L. He, S. K. Özdemir, J. Zhu, W. Kim, and L. Yang, "Detecting single viruses and nanoparticles using whispering gallery microlasers," Nat. Nanotechnol. **6**(7), 428–432 (2011).
5. S. Arnold, D. Keng, S. I. Shopova, S. Holler, W. Zurawsky, and F. Vollmer, "Whispering Gallery Mode Carousel--a photonic mechanism for enhanced nanoparticle detection in biosensing," Opt. Express **17**(8), 6230–6238 (2009).
6. Y.-Z. Yan, C.-L. Zou, S.-B. Yan, F.-W. Sun, J. Liu, C.-Y. Xue, Y.-G. Zhang, L. Wang, W.-D. Zhang, and J.-J. Xiong, "Robust spot-packaged microsphere-taper coupling structure for in-line optical sensors," IEEE Photonics Technol. Lett. **23**(22), 1736–1738 (2011).
7. G. S. Murugan, M. N. Zervas, Y. Panitchob, and J. S. Wilkinson, "Integrated Nd-doped borosilicate glass microsphere laser," Opt. Lett. **36**(1), 73–75 (2011).
8. S. Y. Chen, T. Sun, K. T. V. Grattan, K. Annapurna, and R. Sen, "Characteristics of Er and Er–Yb–Cr doped phosphate microsphere fibre lasers," Opt. Commun. **282**(18), 3765–3769 (2009).
9. G. Nunzi Conti, A. Chiasera, L. Ghisa, S. Berneschi, M. Brenci, Y. Dumeige, S. Pelli, S. Sebastiani, P. Feron, M. Ferrari, and G. C. Righini, "Spectroscopic and lasing properties of Er3+ doped glass microspheres," J. Non-Cryst. Solids **352**(23-25), 2360–2363 (2006).

#274576 http://dx.doi.org/10.1364/OE.24.026956
Journal © 2016 Received 26 Aug 2016; revised 30 Sep 2016; accepted 30 Sep 2016; published 11 Nov 2016

Optics EXPRESS

10. K. Miura, K. Tanaka, and K. Hirao, "CW laser oscillation on both the 4F3/2 –4I11/2 and 4F3/2–4I13/2 transitions of Nd^{3+} ions using a fluoride glass microsphere," J. Non-Cryst. Solids **213–214**, 276–280 (1997).
11. J. M. Ward, P. Féron, and S. N. Chormaic, "A taper-fused microspherical laser source," IEEE Photonics Technol. Lett. **20**(6), 392–394 (2008).
12. M. C. Falconi, G. Palma, F. Starecki, V. Nazabal, J. Troles, S. Taccheo, M. Ferrari, and F. Prudenzano, "Design of an efficient pumping scheme for Mid-IR Dy3+:Ga5Ge20Sb10S65 PCF fiber laser," IEEE Photonics Technol. Lett. **28**(18), 1984–1987 (2016).
13. G. R. Elliott, D. W. Hewak, G. S. Murugan, and J. S. Wilkinson, "Chalcogenide glass microspheres; their production, characterization and potential," Opt. Express **15**(26), 17542–17553 (2007).
14. C. Grillet, S. N. Bian, E. C. Magi, and B. J. Eggleton, "Fiber taper coupling to chalcogenide microsphere modes," Appl. Phys. Lett. **92**(17), 171109 (2008).
15. G. Palma, P. Bia, L. Mescia, T. Yano, V. Nazabal, J. Taguchi, A. Moréac, F. Prudenzano, "Design of fiber coupled Er3+: chalcogenide microsphere amplifier via particle swarm optimization algorithm," Opt. Eng. **53**(7), 071805 (2013).
16. G. Palma, C. Falconi, V. Nazabal, T. Yano, T. Kishi, T. Kumagai, M. Ferrari, and F. Prudenzano, "Modeling of Whispering Gallery Modes for rare earth spectroscopic characterization," IEEE Photonics Technol. Lett. **27**(17), 1861–1863 (2015).
17. A. Giaquinto, L. Mescia, G. Fornarelli, and F. Prudenzano, "Particle swarm optimization-based approach for accurate evaluation of upconversion parameters in Er^{3+}-doped fibers," Opt. Lett. **36**(2), 142–144 (2011).
18. L. Mescia, A. Giaquinto, G. Fornarelli, G. Acciani, M. De Sario, and F. Prudenzano, "Particle swarm optimization for the design and characterization of silica-based photonic crystal fiber amplifiers," J. Non-Cryst. Solids **357**(8–9), 1851–1855 (2011).
19. C. A. Coello Coello, G. T. Pulido, and M. S. Lechuga, "Handling multiple objectives with particle swarm optimization," IEEE Trans. Evol. Comput. **8**(3), 256–279 (2004).
20. F. Prudenzano, L. Mescia, A. D'Orazio, M. De Sario, V. Petruzzelli, A. Chiasera, and M. Ferrari, "Optimization and characterization of rare earth doped photonic crystal fiber amplifier using genetic algorithm," J. Lightwave Technol. **25**(8), 2135–2142 (2007).
21. L. Mescia, P. Bia, M. De Sario, A. Di Tommaso, and F. Prudenzano, "Design of mid-infrared amplifiers based on fiber taper coupling to erbium-doped microspherical resonator," Opt. Express **20**(7), 7616–7629 (2012).
22. L. Mescia, P. Bia, O. Losito, and F. Prudenzano, "Design of Mid-IR Er^{3+}-doped microsphere laser," IEEE Photonics J. **5**(4), 1501308 (2013).
23. F. Prudenzano, L. Mescia, L. Allegretti, V. Moizan, V. Nazabal, and F. Smektala, "Theoretical study of cascade laser in erbium-doped chalcogenide glass fibers," Opt. Mater. **33**(2), 241–245 (2010).
24. V. Moizan, V. Nazabal, J. Troles, P. Houizot, J.-L. Adam, F. Smektala, G. Gadret, S. Pitois, J.-L. Doualan, R. Moncorgé, and G. Canat, "Er^{3+}-doped GeGaSbS glasses for Mid-IR fibre laser application: Synthesis and rare earth spectroscopy," Opt. Mater. **31**(1), 39–46 (2008).
25. K. Kadono, T. Yazawa, S. Jiang, J. Porque, B.-C. Hwang, and N. Peyghambarian, "Rate equation analysis and energy transfer of Er^{3+}-doped Ga_2S_3–GeS_2–$La2S_3$ glasses," J. Non-Cryst. Solids **331**(1-3), 79–80 (2003).
26. S. Girard, L. Mescia, M. Vivona, A. Laurent, Y. Ouerdane, C. Marcandella, F. Prudenzano, A. Boukenter, T. Robin, P. Paillet, V. Goiffon, M. Gaillardin, B. Cadier, E. Pinsard, M. Cannas, and R. Boscaino, "Design of radiation-hardened rare-earth doped amplifiers through a coupled experiment/simulation approach," J. Lightwave Technol. **31**(8), 1247–1254 (2013).
27. B. E. Little, J. P. Laine, and H. A. Haus, "Analytic theory of coupling from tapered fibers and half-blocks into microsphere resonators," J. Lightwave Technol. **17**(4), 704–715 (1999).
28. B. E. Little, S. T. Chu, H. A. Haus, J. Foresi, and J. P. Laine, "Microring resonator channel dropping filters," J. Lightwave Technol. **15**(6), 998–1005 (1997).
29. C. Zou, Y. Yang, C. Dong, Y. Xiao, X. Wu, Z. Han, and G. Guo, "Taper-microsphere coupling with numerical calculation of coupled-mode theory," J. Opt. Soc. Am. B **25**(11), 1895–1898 (2008).
30. H. A. Haus, *Waves and Fields in Optoelectronics* (Prentice Hall Inc., 1984).
31. K. Vahala, *Optical Microcavities* (World Scientific Publishing, 2004).
32. M. J. F. Digonnet, *Rare Earth-Doped Fiber Lasers and Amplifiers* (Marcel Dekker Inc., 2001).

1. Introduction

Whispering Gallery Modes (WGMs) confined in dielectric microspheres can be employed for high performance sensing. Both absorption-based approach, requiring evanescent electromagnetic field coupling to selected WGMs and fluorescence-based technique have been largely used in bio-detection [1–5]. The physical parameters of the medium/background surrounding the microsphere can be efficiently monitored. These applications promise novel sensing systems for label-free chemical/biological monitoring. In [6], Yan et al. propose a packaged structure for the microsphere-taper coupling system. It was constructed by encapsulating the coupling region with a suitable polymer. The spot-packaged structure, integrated with a standard fiber, is an example of feasible structure which could be

Optics EXPRESS

engineered. Microspheres of silica, tellurite, phosphate and ZBLAN glasses, doped with rare earths, have been fabricated, providing low threshold lasing and comb-like emission with extremely narrow linewidth [7–12]. The employment of novel materials, e.g. chalcogenide glasses, could allow novel applications in the medium infrared wavelength range, such as active and passive sensing [13,14].

In [15], Palma et al. used the particle swarm optimization (PSO) approach in order to optimize a mid-IR amplifier constituted by an Er^{3+}-doped microsphere coupled to a tapered fiber. The microsphere and the tapered fiber were made of chalcogenide $Ga_5Ge_{20}Sb_{10}S_{65}$ glass. The PSO procedure was proposed for both the design of the amplifier [15] and, in principle, to recover the unknown spectroscopic parameters of the microsphere glass, i.e. for characterization [16].

The PSO procedure employed for characterization is here indicated with the acronym CPSO (Characterization PSO problem). CPSO approach could be employed, more in general, for sensing chemical compounds/mixture or biomolecules lying in the environment around the microsphere or within a microbubble. However, CPSO drawbacks and critical points related to the fabrication of microsphere and tapered optical fiber could rise. In particular, the uncertainty on the taper and microsphere geometry or gap between the microsphere and the fiber taper could dramatically complicate the CPSO employment.

In this paper, the device fabrication tolerance and a number of practical aspects are accurately investigated. As example of application, an erbium doped chalcogenide glass microsphere coupled to a fiber taper has been considered for spectroscopic measurements. The system feasibility is theoretically demonstrated via a self-consistent approach. In particular, we propose for the first time to use the CPSO twice (double-step CPSO) in order to perform reliable measurements. At first, CPSO is used for an accurate evaluation of the geometrical parameters of the set-up constituted by the fiber taper coupled to a microsphere. Then, CPSO is used for the recovery (evaluation) of the spectroscopic parameters of the microsphere made of rare earth doped glass. The double-step CPSO allows extremely accurate and precise recovering of spectroscopic parameters.

The strength of the proposed double-step CPSO procedure lies in the use of simple output signal measurements as basis data for accurate and low cost recovery of both the set-up geometrical parameters and the unknown rare earth parameters. This novel approach is very promising and can be generalized to other rare earths or to different sensing set-ups (including microbubbles) for detection of various analytes. It is feasible also with reference to label-free chemical detection. The high efficiency of the double-step CPSO is due to the interaction of the WGM resonant modes with the medium, for very long effective lengths, combined with the PSO global search method which is applied for the geometry parameter identification before the physical characterization.

2. Theory

The PSO procedure is a global search numerical method [15–20], it is described in Appendix A. The tentative solutions are represented by the positions $\overline{\boldsymbol{p}}_j$ of the N_b particles (swarm) with velocities $\mathbf{v}_j$ in a search space (solution domain) updated by the algorithm in order to optimize an objective function (fitness). The movement of each particle depends on three factors: i) the cognitive factor, related to the location in the solution space corresponding to the best value of objective function for the considered particle (personal best position $\overline{\boldsymbol{p}}^{PB}$), ii) the social factor, related to the location corresponding to the best value of objective function for the whole swarm (global best position $\overline{\boldsymbol{p}}^{GB}$), iii) the inertial factor, i.e. a suitable resistance to the change of the particle direction. Each of these factors is weighted by an ad hoc parameter: the cognitive parameter c_1, the social parameter c_2, the inertia weight I_w. The PSO procedure ends when a suitable convergence criterion is satisfied. The global best

Optics EXPRESS

position $\overline{\boldsymbol{p}}^{GB}$ is the optimized solution, i.e. the position where the fitness is maximized or minimized (optimized).

In this paper, a reference sensing system (RSS) constituted by a fiber taper coupled to an erbium doped microsphere is designed. In the amplifier, the evanescent field of the optical fiber propagation modes tunnels in the microsphere via the taper. Therefore, the excitation of WGMs is achieved. The interaction of both pump and signal beams with the rare earth doped glass allows the signal optical amplification. The simulation of the RSS is based on the model illustrated in Appendix B [21,22].

More generally, the RSS could be an arbitrary sensing set-up for which the output characteristics can be directly measured. The CPSO algorithm recovers the RSS parameters in order to obtain a sensing set-up model matching the measured output characteristics (data). The CPSO procedure is divided in two steps: G) geometrical and S) spectroscopic characterization. In the first one, G), the CPSO is used for an accurate evaluation of the RSS sizes. In G) the RSS is considered as a passive system, i.e. the interaction of light with rare earth is neglected. The geometrical dimensions obtained in this first step G) are used in the next step S) in order to recover the spectroscopic parameters. In this second step, S), the CPSO is applied for the characterization of the rare earth doped glass, therefore the interaction of light with rare earth is considered. The lifetimes, the up-conversion coefficients and the branching ratio are recovered.

The CPSO fitness function Φ_C, which must be minimized, is defined in Eq. (1):

$$\Phi_C\left(\overline{\boldsymbol{p}}_j\right)=\sum_{k=1}^{N_p}\left(RC_k-RC_{CPSO,k}^{j}\right)^2, \tag{1}$$

with $j=1,2,\ldots,N_b$, $k=1,2,\ldots,N_p$. RC_k is the *k-th* measured RSS output characteristic. In particular, i) for the passive microsphere characterization, RC_k is the output signal power $S_{p,k}^{out}$, as a function of the wavelength, obtained for the *k-th* input signal power $S_{p,k}$; ii) for the active microsphere behaviour, RC_k is the optical gain g_k obtained for the *k-th* input pump power P_p. We underline that in actual sensing set-ups RC_k can be directly measured via an optical detector. In this paper, it is simulated by considering the RSS model with nominal geometrical and measured spectroscopic parameters. $RC_{CPSO,k}^{j}$ is the output characteristic (output signal power in passive model or gain in active model) simulated for the *j-th* particle of the swarm, i.e. calculated in the *j-th* particle position within the solution space.

The CPSO algorithm and the set-up, comprising the tapered fiber coupled to the microsphere, constitute the proposed tool for rare earth characterization. R_{CPSO} is the number of the different CPSO executions. The weighted mean WM_{GBP} of the CPSO global best positions, evaluated by considering all the R_{CPSO} performed executions, is calculated by means of Eq. (2):

$$WM_{GBP}=\frac{\sum_{r=1}^{R_{CPSO}}\left(\overline{\boldsymbol{p}}_r^{GB}\times\frac{1}{\Phi_c\left(\overline{\boldsymbol{p}}_r^{GB}\right)}\right)}{\sum_{r=1}^{R_{CPSO}}\frac{1}{\Phi_c\left(\overline{\boldsymbol{p}}_r^{GB}\right)}}, \tag{2}$$

where $\Phi_c\left(\overline{\boldsymbol{p}}_r^{GB}\right)$ is the global best fitness, i.e. the fitness calculated in the global best position $\overline{\boldsymbol{p}}_r^{GB}$ for the *r-th* CPSO execution, with $r=1,2,\ldots,R_{CPSO}$. The reciprocal of the global

Optics EXPRESS

best fitness is used as weight in mean calculation because a smaller fitness value corresponds to a better CPSO performance.

In order to investigate the goodness of the proposed method, the percentage error between the CPSO recovered parameters, $WM_{GBP,}$ and the V_{nom} nominal/target parameters used in the RSS model for the calculation of RC_k is evaluated. The percentage error, for each parameter, is calculated by Eq. (3):

$$E_{\%} = \frac{|WM_{GBP} - V_{nom}|}{V_{nom}} \cdot 100, \tag{3}$$

This percentage error, if low enough with respect to the physical meaning of the recovered parameter, validates the proposed approach.

3. Electromagnetic design of the set-up and simulated results

For the modeling of the amplifier constituted by the rare earth doped microsphere coupled to the fiber taper, the theory of Appendix B is implemented in a computer code allowing the calculation of the optical gain. The details are reported in [21,22].

3.1 Design of the reference sensing system RSS

The pump wavelength is close to λ_p = 980 nm and the signal wavelength is close to λ_s = 2770 nm. In order to carry out a realistic gain calculation, the simulations are performed by considering measured spectroscopic parameters of an Er^{3+}:$Ga_5Ge_{20}Sb_{10}S_{65}$ glass sample. The refractive index wavelength dispersion is modelled by means of the Cauchy equation, with measured spectroscopic parameters reported in Table 1 [21–24], λ being the wavelength expressed in microns. The simulation is carried out by varying the parameter n of $WGM_{l,m,n}$ from 1 to 3 and by imposing $l = m$ (fundamental mode). WGMs with $l \neq m$ are neglected because they exhibit low overlapping factor $\Omega_{l,m,n}^{q,s}$, see Appendix B [21]. WGMs competition, i.e. their amplification or attenuation, strongly depends on the absorption and emission cross sections at their peculiar resonant wavelength.

Table 1. Spectroscopic Parameters of the Er^{3+}-doped Chalcogenide Glass [21–24]

Cauchy Equation	$n(\lambda) = 2.2181 + \frac{0.0551}{\lambda^2} - \frac{0.0003}{\lambda^4}$		
Cross-relaxation and up-conversion coefficients	Value		
$C_3\left[\mathrm{m}^3/\mathrm{s}\right]$	$2 \cdot 10^{-23}$		
$C_{up}\left[\mathrm{m}^3/\mathrm{s}\right]$	$3 \cdot 10^{-23}$		
$C_{14}\left[\mathrm{m}^3/\mathrm{s}\right]$	$5 \cdot 10^{-24}$		
Energy level transitions	Wavelength [nm]	Lifetime [ms]	Branching ratio [%]
$^4I_{13/2} \rightarrow {}^4I_{15/2}$	1532	$\tau_2 = 1.83$	$\beta_{21} = 100.0$
$^4I_{11/2} \rightarrow {}^4I_{15/2}$	986	$\tau_3 = 1.37$	$\beta_{31} = 86.28$
$^4I_{11/2} \rightarrow {}^4I_{13/2}$	2771	$\tau_3 = 1.37$	$\beta_{32} = 13.72$
$^4I_{9/2} \rightarrow {}^4I_{15/2}$	810	$\tau_4 = 1.08$	$\beta_{41} = 80.38$
$^4I_{9/2} \rightarrow {}^4I_{13/2}$	1719	$\tau_4 = 1.08$	$\beta_{42} = 18.82$
$^4I_{9/2} \rightarrow {}^4I_{11/2}$	4529	$\tau_4 = 1.08$	$\beta_{43} = 0.80$
$^4F_{9/2} \rightarrow {}^4I_{15/2}$	663	$\tau_5 = 0.13$	$\beta_{51} = 91.99$
$^4F_{9/2} \rightarrow {}^4I_{13/2}$	1168	$\tau_5 = 0.13$	$\beta_{52} = 4.32$
$^4F_{9/2} \rightarrow {}^4I_{11/2}$	2019	$\tau_5 = 0.13$	$\beta_{53} = 3.34$
$^4F_{9/2} \rightarrow {}^4I_{9/2}$	3623	$\tau_5 = 0.13$	$\beta_{54} = 0.35$

Optics EXPRESS

Therefore, the different emission and absorption cross section values are accurately taken into account for the modelling of the $WGM_{l,m,n}$ resonating at different wavelengths. The absorption cross section at the pump wavelength λ = 980 nm is close to 1.32 × 10^{-24} m^2, while the emission and absorption cross sections at the signal wavelength λ = 2770 nm are close to 1.4 × 10^{-24} m^2 and 1.23 × 10^{-24} m^2, respectively. The thickness of the erbium-doped region (close to the microsphere surface) and the erbium concentration are h_{Er} = 3 μm and C_{Er} = 0.5 w%, respectively.

A reference sensing system RSS is designed with the aim of obtaining feasible geometrical parameters maximizing the amplifier optical gain g. The microsphere radius ρ_0, the taper waist radius W_T, the taper angle α and the taper-microsphere gap G are designed by considering these technological needs: i) a suitable microsphere radius in order to have resonance at both the pump and signal wavelengths; ii) the waist radius larger than the inferior limit W_T = 0.5μm, since chalcogenide glass exhibits a number of drawbacks in the construction of taper having smaller waist; iii) the waist radius smaller than the superior limit W_T = 1μm in order to have single-mode propagation; iv) feasible taper angle; v) feasible taper–microsphere gap. The designed geometrical parameters are reported in Table 2. The input pump power is P_p = 100 mW and the input signal power is S_p = –50dBm. The data in Table 1 and 2 and the computer code based on theory of Appendix B allow the simulation of RC_k values to be used in Eq. (1). These values should be measured in actual sensing set-ups. Ten different resonating WGMs are simulated in the RSS. In Table 3, the main characteristics of these resonating modes are reported. The resonance wavelength λ_r, the modal parameters l, m and n, the optical gain g and the intrinsic quality factor Q [21] for each WGM mode are listed. In particular, the signal WGM maximizing the amplifier gain g has modal order n = 1; l = m = 117 at the wavelength λ_s ≈2760 nm; the WGM at the pump wavelength has modal order n = 1, l = m = 349 at the wavelength λ_p ≈981 nm.

Table 2. RSS Design Parameters

Parameters	RSS value
Microsphere radius ρ_o [μm]	24.8
Taper waist radius W_T [μm]	1.0
Taper – microsphere gap G [μm]	0.5
Taper angle α [rad]	0.04

Table 3. WGM Characteristics of RSS at Signal Wavelength λ_r

WGM resonance wavelength λ_r [nm]	$l = m$ parameter	n parameter	Optical gain g [dB]	Quality factor Q [$\cdot 10^7$]
2806	115	1	4.02	9.06
2783	116	1	5.66	9.10
2760	117	1	8.34	9.14
2809	108	2	2.19	8.75
2785	109	2	3.17	8.79
2762	110	2	4.76	8.84
2819	102	3	2.84	8.47
2795	103	3	3.65	8.52
2771	104	3	4.97	8.56
2747	105	3	4.44	8.61

Preliminary investigations on the RSS showed that the effect of the cross-relaxation parameter C_{14} ($^4I_{15/2}$, $^4I_{9/2}$) → ($^4I_{13/2}$, $^4I_{13/2}$) on the gain calculation is negligible. Similarly, the ion lifetime τ_4 related to the transition $^4I_{9/2}$ → $^4I_{15/2}$, if varied in the range [0.8 ms ÷ 1.3 ms], does not cause significant RSS gain changes. Therefore, the recovery of C_{14} and τ_4 is not considered as CPSO goal.

Optics EXPRESS

3.2 Sensitivity of gain to fabrication tolerance and to rare earth coefficients

The sensitivity of the calculated optical gain g to the dimensions variation of the RSS is evaluated. The gain g is calculated as the ratio between the optical powers at the fiber ends, including the coupling/interaction with rare earth microsphere, see Eq. (13), Appendix B.

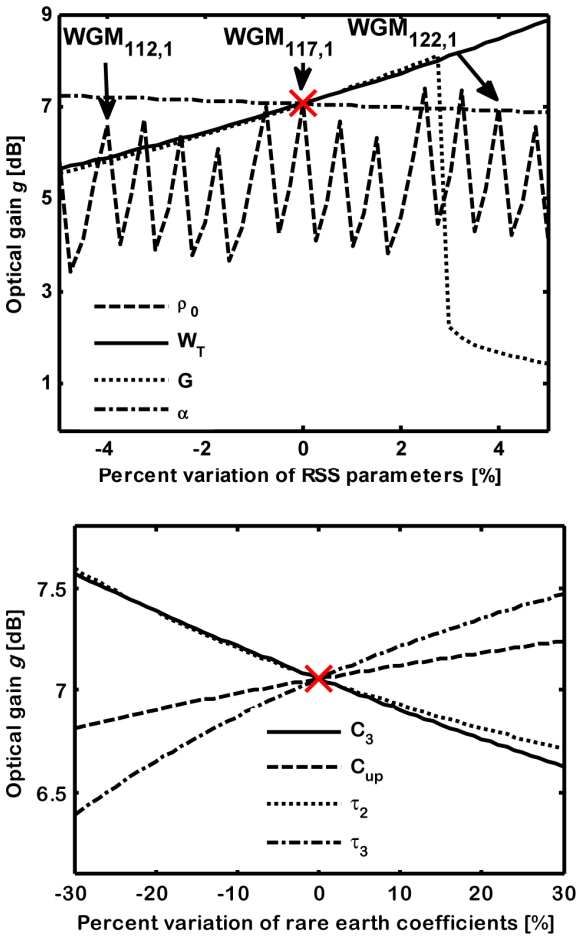

Fig. 1. (a).Simulated optical gain g versus the RSS geometrical parameters. For each curve, only the parameter specified in the legend is varied, the other parameters have the nominal values of Tables 1 and 2. Input pump power P_p = 140mW, input signal power S_P = –50dBm. (b) Simulated optical gain g versus the rare earth coefficients. For each curve, only the coefficient specified in the legend is varied, the other parameters have the nominal values of Table 1 and 2. Input pump power P_p = 140 mW, input signal power S_p = - 50dBm.

Figure 1(a) reports the optical gain g as a function of the percent variation of the geometrical dimensions. For each curve, only the geometrical parameter specified in the legend is changed, while the others have the nominal values reported in Table 1 and 2. The red cross represents the RSS gain obtained by using nominal values for all the geometrical parameters. This reference optical gain is g = 7.06 dB, obtained with input pump power P_p = 140 mW and input signal power S_p = –50 dBm. In Fig. 1(a) it is apparent that small percent variations of geometrical parameters strongly affect the calculated optical gain g. A variation of the microsphere radius ρ_0 (dashed curve) causes the variation of the guided WGM. For the sake of conciseness, in Fig. 1(a) only three resonating $WGM_{l=m,n}$ are indicated. Changes in the calculated gain g are caused by the variation of the waist radius W_T (full curve) or the gap

Optics EXPRESS

G (dotted curve) in the range [-5% ÷ 3%]. A decrease of the waist radius W_T causes an increase in the fiber evanescent field and therefore a strongest coupling between microsphere and fiber. A coupling increase can be also obtained by decreasing the gap G. If the gap G increases more than 3%, the optical gain drastically decreases because the coupling becomes too weak and the inversion of rare earth ion population is not reached.

The change of taper angle α (dash-dotted curve) has a very slight effect on the calculated optical gain. In fact, a variation of taper angle $\Delta\alpha = \pm 5\%$ causes a negligible change of the simulated optical gain, close to $\Delta g = \pm 2.5\%$. In the actual case, the uncertainty on taper angle is of about $\Delta\alpha = \pm 5\%$. Therefore, in this paper the taper angle α is not considered in CPSO recovery. Figure 1(a) demonstrates that the model can be sensitive to the variations of microsphere radius ρ_0, taper waist radius W_T and taper-microsphere gap G. This result is worthwhile since the fabrication tolerance is about 10% for all the aforesaid parameters.

Figure 1(b) reports the optical gain g as a function of the percent variation of the rare earth coefficients. For each curve only the rare earth coefficient specified in the legend is changed while the other parameters have the nominal values reported in Table 1 and 2. The red cross represents the RSS gain obtained by using nominal values for all the rare earth parameters. The reference optical gain is $g = 7.06$ dB, obtained with input pump power $P_p = 140$ mW and input signal power $S_p = -50$ dBm. The simulated gain g depends on the change of rare earth coefficients. The gain variation due to the change of rare earth coefficient C_{up} is slighter than that occurring for the other parameter fluctuations.

4. CPSO characterization

Before applying the CPSO procedure, the RSS gain g_k, $k = 1,\ldots,N_P$, is simulated for the input signal power $S_P = -50$dBm and for different input pump powers P_p . In particular, $N_p = 7$ pump powers linearly spaced in the range $P_p = [20 \div 140]$mW are considered. The geometrical and spectroscopic parameters have the nominal values reported in Table 1 and 2.

The calculated gain g_k, (circles) versus the input pump power are reported in Fig. 2, the full curve linearly interpolates the simulated points. The N_p input pump powers showed in Fig. 2 are arbitrarily chosen. In the actual case, after the set-up design and fabrication, the RSS optical gain g_k values can be easily measured.

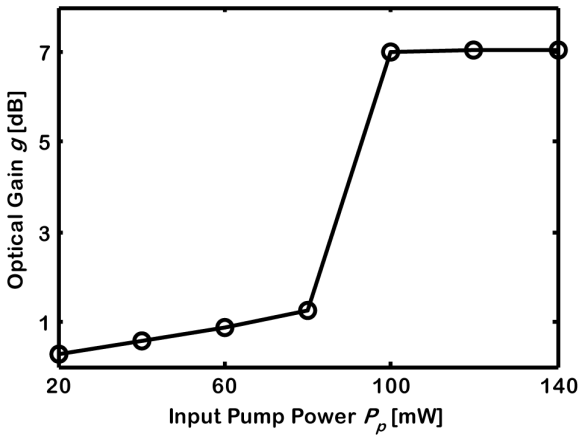

Fig. 2. Calculated RSS optical gain g_k versus the input pump powers P_p. Input signal power is $S_P = -50$ dBm. The geometrical and spectroscopic parameters are reported in Table 1 and 2.

In CPSO procedure, the cognitive parameter is $c_1 = 1.494$, the social parameter is $c_2 = 1.494$, the inertia weight I_w is a vector with I_{PSO} elements linearly spaced from 0.4 to 0.9. The reflecting walls boundary conditions are used, i.e. the particles that hit the boundary of solution space are reflected backward [19]. PSO algorithm is characterized by a very high

Optics EXPRESS

convergence speed. In some cases, this can be a problem because the PSO could converge in a local minimum/maximum. In order to reduce convergence speed, a mutation operator is introduced. This operator modifies in a stochastic way the positions of the particles [19]T.

For a comparison between single and double-step CPSO, when the geometry uncertainty is taken into account, the geometrical and the rare earth parameters are simultaneously recovered. Therefore, the simulation reported in the following does not refer to the double-step CPSO; it is performed via a single CPSO. The nominal values in Table 1 and 2 represent the target values of CPSO procedure. The up-conversion coefficients C_{up} and C_3 and the values of ion lifetimes τ_2 and τ_3 are CPSO recovered.

CPSO fitness function Φ_{SC}, to be minimized, is derived by Eq. (1). It is expressed as a function of the optical gain g_k of the amplifier, see Eq. (4):

$$\Phi_{SC}\left(\bar{\boldsymbol{p}}_j\right)=\sum_{k=1}^{N_p}\left(g_k-g_k^j\right)^2, \tag{4}$$

with $j=1,2,\ldots,N_b$, $k=1,2,\ldots,N_p$. g_k is the optical gain of the RSS illustrated in Fig. 2, g_k^j is the optical gain g_k for the *j-th* particle of the swarm and the *k-th* pump power.

The single CPSO does not allow an accurate geometrical and spectroscopic parameter recovery. For example, spectroscopic values are affected by large errors, $E_{\%}\approx 30\%$, for the up-conversion coefficients C_{up} and C_3 and $E_{\%}\approx 50\%$ for the ion lifetimes τ_2 and τ_3. In fact, the increase of the parameter number to be simultaneously recovered makes the algorithm convergence critical. Moreover, the computational cost increases exponentially. On the other hand, the method suggested in [16], if the geometry uncertainty is realistically considered, is not completely reliable.

4.1 Double-step CPSO: G) geometrical characterization

The alternative approach is here illustrated. The problem is solved in two subsequent steps: i) geometrical characterization G) and ii) rare earth spectroscopic characterization S). In G) the recovered parameters are the microsphere radius ρ_0, taper waist radius W_T and taper-microsphere gap G. In order to neglect the rare earth - light interaction, the pump at $\lambda_p \approx 981$ nm is not considered (it is set equal to zero). Without optical pump power, the erbium level $^4I_{11/2}$ is depopulated and there is not optical gain.

In the geometrical characterization, the fitness function $\Phi_{GC}\left(\bar{\boldsymbol{p}}_j\right)$ is given by Eq. (5). It is derived by Eq. (1):

$$\Phi_{GC}\left(\bar{\boldsymbol{p}}_j\right)=\left(S_p^{out}-S_{p,CPSO}^{out,j}\right)^2, \tag{5}$$

with $j=1,2,\ldots,N_b$. S_p^{out} is the RSS output signal power versus the wavelength, for the signal input power S_p = 100 mW, the other parameters are listed in Table 1 and 2. $S_{p,CPSO}^{out,j}$ is the output signal power simulated for the *j*-th particle.

The RSS output signal power S_p^{out} versus the wavelength is depicted in Fig. 3, it is used in the fitness function $\Phi_{GC}\left(\bar{\boldsymbol{p}}_j\right)$ calculation. The ten dips in Fig. 3 refer to the ten WGM resonances listed in Table 3. The modal order $l = m$, n is reported for all the dips. The dashed RSS output signal power corresponds to WGM having modal order $l = m = 117$, $n = 1$, which allows the highest amplification in active behavior (it will be considered in the next section).

In the case of geometrical characterization, the CPSO suitable maximum iteration number is I_{PSO} = 50 and the number of particles is N_b = 50. The space dimension is D = 3 and the position vector is $\bar{\boldsymbol{p}}_j=\left[\rho_o^j, W_t^j, G^j\right]$, with $j=1,2,\ldots,N_b$. For each parameter, the solution

Optics EXPRESS

domain is chosen in agreement with the fabrication process tolerance (about 10%). $R_{CPSO} = 20$ CPSO executions are performed. The weighted mean WM_{GBP} is calculated via Eq. (2), by choosing, among the 20 executions, the five global best positions $\overline{\boldsymbol{p}}^{GB} = \left[\rho_o^{GB}, W_t^{GB}, G^{GB} \right]$ with lower global best fitness.

Table 4 reports the RSS target values, the solution domains, the CPSO recovered weighted mean WM_{GBP} values, the percent error $E_{\%}$ and the CPSO standard deviation SD for each parameter.

The recovered values are in excellent agreement with the target values. The reason is apparent: the microsphere radius ρ_0 is strictly related to the resonant wavelengths λ_s where the dips of Fig. 3 occur. CPSO can recover the microsphere radius with a negligible error close to $E_{\%} = 1 \times 10^{-8}\%$, so the three-dimensional solution space ($D = 3$) becomes very close to a bi-dimensional ($D = 2$) one, making easier the problem solution.

It is worthwhile to note that the percent error $E_{\%}$ on the recovered taper radius W_T and gap G have similar absolute value but opposite sign. This behavior is observed not only for the weighted mean WM_{GBP}, but also in each CPSO execution and agrees with Fig. 1(a).

In the next section, the recovered geometry is used in order to perform the rare earth characterization.

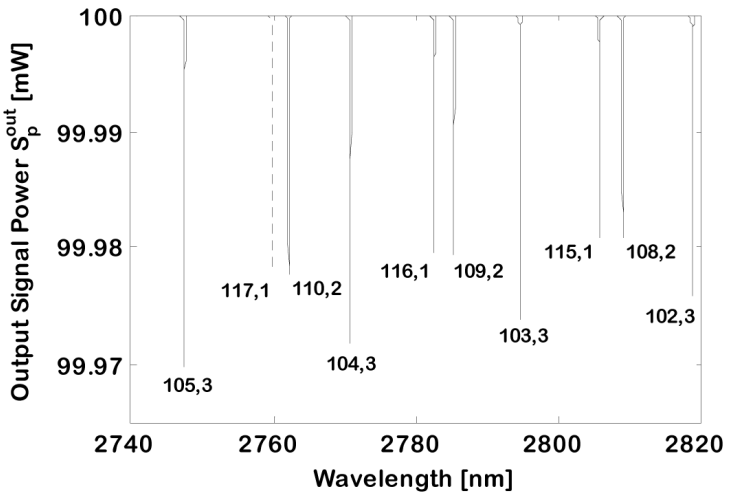

Fig. 3. RSS output signal power S_p^{out} versus the wavelength. Input signal power $S_p = 100$ mW

Optics EXPRESS

Table 4. Geometrical G) Characterization

Variable	ρ_0 [μm]	W_T [μm]	G [μm]
Target Value	24.8	1	0.5
Solution Domain Ranges	24.7 ÷ 24.9	0.9 ÷ 1.1	0.4 ÷ 0.6
WM_{GBP}	24.8	0.9997	0.5002
SD	$1.7 \cdot 10^{-7}$	$9.9 \cdot 10^{-4}$	$4.1 \cdot 10^{-4}$
Percent Error $E_{\%}$ [%]	0%	–0.03%	0.03%

4.2 Double-step CPSO: S) Rare earth characterization

In the second step, the optical pump power is used in order to activate the interaction between light and rare earth ions and simulate the amplifier gain g_k. This allows the spectroscopic characterization, the geometrical parameters being identified in the previous section. In CPSO – I case, the up-conversion coefficients C_{up} and C_3 and the lifetimes τ_2 and τ_3 are the unknown parameters. Very large solution domains are taken into account in order to test the method robustness. Typical measurement uncertainty on lifetimes is about 5-10% (using Judd-Ofelt theory), about 30% on up-conversion coefficient C_{up} and about 20% on C_3 (estimated by fitting the simulated decay curves to the measured ones [25]).

In S) CPSO problem, the fitness function Φ_{SC}, which must be minimized, is defined in Eq. (4). The considered input pump powers are showed in Fig. 2. After a preliminary investigation, the CPSO suitable maximum iteration number and the number of particles are I_{PSO} = 50 and N_b = 40 respectively. The space dimension is D = 4 and the position vector is $\overline{\boldsymbol{p}}_j = \left[C_{up}{}^j, C_3{}^j, \tau_2{}^j, \tau_3{}^j \right]$, with $j = 1, 2, \ldots, N_b$. R_{CPSO} = 10 different CPSO executions are performed.

Figure 4 shows the global best positions in the C_3-C_{up} and τ_2- τ_3 solution domains for the ten CPSO executions (dots), the target values (circles) and the weighted mean WM_{GBP} (cross) calculated using Eq. (2) and reported in Table 5. The high C_{up} dispersion, i.e. the large standard deviation, is originated, as expected, from the low RSS sensitivity to this parameter change. The WM_{GBP} calculation allows the recovery of C_{up} parameter very close to the target one in spite of the large dispersion.

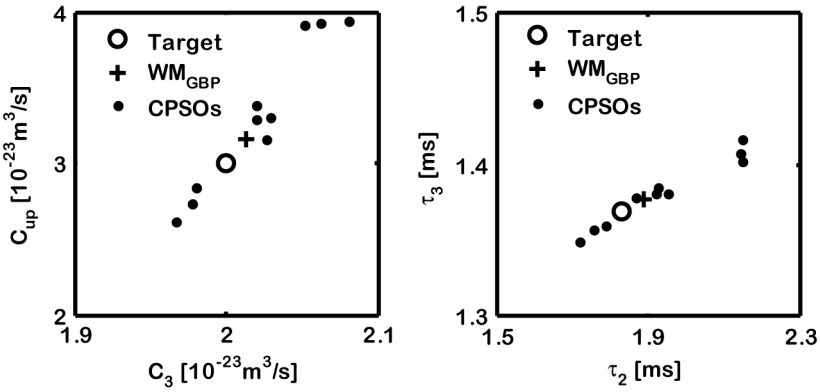

Fig. 4. Position in C_3-C_{up} and τ_2-τ_3 solution domains of the global best positions (dots) recovered via the R_{CPSO} = 10 CPSO executions, the target values (circles) and the weighted means WM_{GBP} reported in Table 5 (crosses).

Optics EXPRESS

Table 5. Spectroscopic Characterization, S) CPSO – I case

Variable	C_3 $[\cdot 10^{-23}\ m^3/s]$	C_{up} $[\cdot 10^{-23}\ m^3/s]$	τ_2 $[ms]$	τ_3 $[ms]$
Target Value	2	3	1.83	1.37
Solution Domain Ranges	1 ÷ 3	2 ÷ 4	0.1 ÷ 3	0.1 ÷ 3
WM_{GBP}	2.01	3.16	1.89	1.38
SD	0.04	0.47	0.15	0.02
Percent Error $E_{\%}$	0.64%	5.49%	3.39%	0.52%

Table 5 reports the solution domain, the recovered weighted mean WM_{GBP}, the percent error $E_{\%}$ and the CPSO standard deviation SD for each parameter, S) CPSO – I case.

The target values and the related CPSO recovered WM_{GBP} are very close. Each of these errors is extremely low and much smaller than the usual measurement uncertainty. In other words, these errors are much smaller than those performed with actual high cost measurement systems. This S) CPSO I-case application shows that, even if i) the search domain is large, ii) the up-conversion coefficients C_{up} and C_3 are not easily measurable, the followed approach allows a very robust characterization. The computation time is about 6 days with an Intel Xeon E5-2620 CPU.

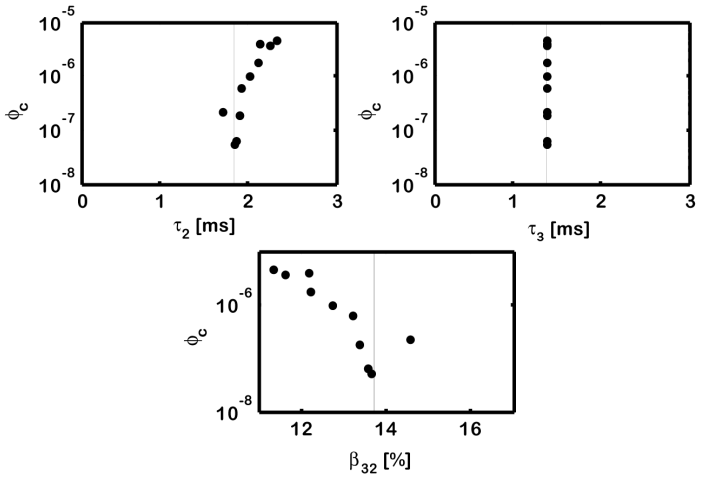

Fig. 5. Fitness function Φ_c (in logarithmic scale) versus τ_2, τ_3 and β_{32} for the global best positions $\overline{\boldsymbol{p}}^{GB}$ recovered by all the R_{CPSO} = 10 executions in S) CPSO-III case. The vertical line represents the target position in each dimension.

In order to further test the method, two other cases are considered. In S) CPSO-II case, the branching ratio β_{32} ($^4I_{11/2} \rightarrow {}^4I_{13/2}$) and the up-conversion coefficients C_{up} and C_3 are recovered. In S) CPSO-III case, the branching ratio β_{32} and the ion lifetimes τ_2 and τ_3 are recovered. For the branching ratio β_{32}, a typical measurement uncertainty is close to 30%. In these S) CPSO cases, the fitness function, which must be minimized, is defined in Eq. (4). The input pump powers used are those of Fig. 2. The CPSO suitable maximum iteration number and the number of particles are I_{PSO} = 50 and N_b = 40, respectively. The space dimension for the both cases is D = 3 and the position vectors are $\overline{\boldsymbol{p}}_j = \left[C_{up}{}^j, C_3{}^j, \beta_{32}{}^j \right]$ and

Optics EXPRESS

$\bar{\boldsymbol{p}}_j = \left[\tau_2^{\,j}, \tau_3^{\,j}, \beta_{32}^{\,j}\right]$, with $j = 1, 2, \ldots, N_b$, for the CPSO-II case and CPSO-III case, respectively.

Figure 5 reports the fitness function Φ_c as defined in (4), in logarithmic scale, versus τ_2, τ_3 and β_{32} for the global best positions $\bar{\boldsymbol{p}}^{GB}$ recovered via the $R_{PSO} = 10$ executions in CPSO-III case. The vertical line represents the target value in each dimension. The global best position with the smallest fitness (about $\Phi_c = 5.4 \cdot 10^{-8}$) corresponds to the best solution among the $R_{PSO} = 10$ executions. In this case the best global solution is defined by the particle position closer to the target (lying on the vertical line) in the three dimensions space. For this particle, the percent error on lifetimes τ_2 and τ_3 and on branching ratio β_{32} are respectively $E_{\%} = 0.78\%$, $E_{\%} = -0.03\%$ and $E_{\%} = -0.54\%$. In other case the minimum of the fitness could occur for particle with recovered parameters slightly more distant from the target ones, as expected in a global search approach. In order to minimize the error made on the single parameter, Eq. (2) is employed for evaluating the weighted mean WM_{GBP}.

Table 6 and Table 7 report the solution domain, the recovered weighted mean WM_{GBP}, the percent error $E_{\%}$ and the CPSO standard deviation SD obtained via $R_{CPSO} = 10$ executions for the CPSO-II case and CPSO-III case, respectively. Table 6 shows that, in the worst case, the largest error $E_{\%} = 0.75\%$ is made on C_{up} parameter recovery. Table 7 shows that, in the worst case, the largest error $E_{\%} = 1.35\%$ is made on τ_2 parameter recovery. The computation time in each case is about 6 days with an Intel Xeon E5-2620 CPU.

The S) CPSO I, II and III cases demonstrate that the proposed approach provide to recover different spectroscopic parameters with errors lower than the typical measurement uncertainties. Moreover, this approach is a solution to avoid the use of expensive measurement instruments since it requires a simple optical detector and a personal computer.

Table 6. Spectroscopic Characterization, S) CPSO – II case

Variable	C_3 [$\cdot 10^{-23}$ m^3/s]	C_{up} [$\cdot 10^{-23}$ m^3/s]	β_{32} [%]
Target Value	2	3	13.72
Solution Domain Ranges	1 ÷ 3	2 ÷ 4	11 ÷ 17
WM_{GBP}	2	3.02	13.78
SD	0.002	0.257	0.49
Percent Error $E_{\%}$	0.05%	0.75%	0.42%

Table 7. Spectroscopic Characterization, S) CPSO – III case

Variable	τ_2 [ms]	τ_3 [ms]	β_{32} [%]
Target Value	1.83	1.37	13.72
Solution Domain Ranges	0.1 ÷ 3	0.1 ÷ 3	11 ÷ 17
WM_{GBP}	1.855	1.369	13.598
SD	0.18	0.002	0.96
Percent Error $E_{\%}$	1.35%	–0.03%	–0.89%

5. Conclusion

WGM resonance and double CPSO approach constitute a solution for complete and robust rare earth characterization based on transmittance/gain measurement. The procedure, in order

Optics EXPRESS

to mitigate the effect of uncertainty on geometrical dimensions, follows two steps. In the first one, the geometrical characterization is performed. In the second step, the spectroscopic parameters are recovered. The largest error in geometrical characterization is on the gap between microsphere and taper fiber and it is 0.03%. The developed characterization tool recovers the spectroscopic parameters with an error less than that provided by high-cost measurement instruments. The errors made on the up-conversion coefficients C_{up} and C_3 and the branching ratio β_{32} are 0.75%, 0.05% and 0.42%, respectively. The method can be applied to other rare earths. Moreover, the same approach can be applied to other sensing systems. For example, the model of the medium surrounding a passive microsphere or of a microbubble, containing a polluted solution or a biological fluid, can be considered. In this case, the parameters to be recovered can be those related to the analyte concentration. They can be evaluated via direct transmittance measurement instead of resonance wavelength-shift one, e.g. performed by employing the optical spectrum analyzer.

6. Appendix A: PSO algorithm

The PSO is a global search numerical method, inspired by the social behavior exhibited by a variety of animals during their search for food, e.g. bees, fishes, birds [17–20]. In PSO algorithm, a population of N_b tentative solutions or particles corresponds to the swarm of bees. The tentative solutions are updated in the multidimensional solution space with the aim of optimizing a suitable fitness function. For a D-dimensional search space, the position of each particle is identified by a D-dimensional vector $\bar{\boldsymbol{p}}_j$, which constitutes the tentative solution (a set of tentative values of the independent variables). The fitness function is optimized (e.g. maximized or minimized) during the execution. Each particle trajectory is updated till the convergence criterion is reached. The particle trajectory depends on i) the location in the solution space where the best fitness value is found by the single particle, called personal best $\bar{\boldsymbol{p}}^{PB}$, and ii) the best location found by the entire swarm, called global best $\bar{\boldsymbol{p}}^{GB}$. The change of the current particle position is obtained by applying a velocity, $\mathbf{v}_j$, which depends on both the personal experience and on the collective experience of the swarm. The velocity of the particle is updated at the n+1 iteration according to the following equation [19]:

$$\mathbf{v}_j(n+1) = \chi \times \left\{ \mathbf{v}_j(n) + c_1 \times r_1 \times \left[\bar{\boldsymbol{p}}_j^{PB}(n) - \bar{\boldsymbol{p}}_j(n) \right] + c_2 \times r_2 \times \left[\bar{\mathbf{p}}^{GB}(n) - \bar{\mathbf{p}}_j(n) \right] \right\}, \quad (6)$$

$$\bar{\boldsymbol{p}}_j(n+1) = \bar{\boldsymbol{p}}_j(n) + \boldsymbol{v}_j(n+1), \quad (7)$$

with $j = 1, 2, \ldots, N_b$.

$$C_F = \frac{2}{\left| 2 - \chi - \sqrt{\chi^2 - 4\chi} \right|}, \quad (8)$$

with $\chi = c_1 + c_2$ and $\chi > 4$.

C_F is the constriction factor, c_1 and c_2 are the cognitive and social parameters respectively, r_1 and r_2 are two random numbers uniformly distributed in the range [0, 1], employed to obtain an efficient search.

7. Appendix B: Model of a rare earth doped microsphere

The modeling of the amplifier is based on electromagnetic mode analysis of both fiber and microsphere, the coupled mode theory [27] and the rate equations describing the rare earth ions behavior. The solution of the scalar Helmholtz equation in spherical coordinates is:

Optics EXPRESS

$$\psi_{l,m,n}(r,\theta,\gamma) = N_s R(r)\Theta(\theta)\Gamma(\gamma), \tag{9}$$

where $\psi_{l,m,n}(r,\theta,\gamma) = E_\theta$, for the transverse electric (TE) modes, $\psi_{l,m,n}(r,\theta,\gamma) = H_\theta$, for the transverse magnetic (TM) modes; N_s is a normalization constant, it is calculated by setting the volume integral of $\psi^2_{l,m,n}$ over all the space, divided by the microsphere circumference, equal to unit [27]. The resonant electromagnetic modes bounded in the microsphere are called Whispering Gallery Modes (WGMs). Each WGM is identified by three integers l, m, n; $l-m+1$ is the number of field maxima in the polar direction $\hat{\theta}$; n is the number of field maxima along the radial direction. The azimuthal dependence $\Gamma(\gamma)$ is expressed via a complex exponential function with argument depending on the mode number m. The approximation $\theta << 1$ for the polar angle has been considered because the predominant WGMs are those coupled via the tapered fiber; the polar dependence $\Theta(\theta)$ is expressed by the Hermite polynomials of order $N = l - m$. The radial solution $R(r)$ is expressed by the spherical Bessel functions depending on the mode orders l and n. The boundary conditions and the matching conditions for the tangential components of the electric and magnetic fields at the sphere/background interface are set and the characteristic equation is written. The solution of the characteristic equation leads to the calculation of the resonance wavelengths and their corresponding modal field distributions.

The coupling of the optical power between the tapered fiber and the microsphere is modeled by using the coupled mode theory [21, 22, 28]. The coupled-mode equations are obtained by considering: weak coupling, small internal resonator losses, small perturbation of optical fiber and resonator modes, slowly varying amplitude approximation, single mode fiber coupled to a WGM of the cavity, adiabatic tapered fiber, coupling region much smaller than the microsphere diameter.

For adiabatic taper, the fiber radius W_T can be expressed as:

$$W_T(z) = W_T(0) + |z|\alpha, \tag{10}$$

where α is the taper angle and $W_T(0)$ is the fiber radius at the waist of the tapered fiber. The z-depending propagation constant, β_f, of the optical fiber mode can be calculated by solving the *z*-dependent characteristic equation [21].

The interaction of the WGMs with the rare earth doped microsphere has been investigated by using the rate equation model. The electronic transitions and the energy transfers of the trivalent erbium ions in the chalcogenide glass have been taken into account, i.e. the ($^4I_{15/2} \rightarrow {}^4I_{11/2}$) pump transition at the wavelength 0.98μm, the ($^4I_{11/2} \rightarrow {}^4I_{13/2}$) stimulated emission transition at the wavelength 2.7μm, the spontaneous energy transfer mechanisms occurring in a pair of Er^{3+} ions, ($^4I_{13/2}$, $^4I_{13/2} \rightarrow {}^4I_{15/2}$, $^4I_{9/2}$), ($^4I_{11/2}$, $^4I_{11/2} \rightarrow {}^4I_{15/2}$, $^4S_{3/2}$), ($^4I_{15/2}$, $^4I_{9/2} \rightarrow {}^4I_{13/2}$), ($^4I_{9/2}$, $^4I_{9/2} \rightarrow {}^4S_{3/2}$, $^4I_{13/2}$), ($^4I_{15/2}$, $^4S_{3/2} \rightarrow {}^4I_{13/2}$, $^4I_{9/2}$), ($^4I_{13/2}$, $^4I_{9/2} \rightarrow {}^4I_{15/2}$, $^4S_{3/2}$).

The WGMs overlap the microsphere doped area, in the plane $\hat{r}\cdot\hat{\theta}$, which is divided in q sectors [21]. The rate equations describing the population dynamic of the ion energy levels are written as function of i) N_i^q, $i = 1,2,...6$ the concentration of *i-th* level in the *q-th* sector; ii) the contribution to the pump and signal rates of each WGM propagating into the microsphere.

The time domain evolution of the amplitude A of the internal cavity electromagnetic field at the pump P and the signal S wavelengths, for the WGM solution identified by *l,m,n*, can be obtained by solving the differential equations [21, 28–32]:

Optics EXPRESS

$$\begin{aligned}\frac{dA^{P}_{l,m,n}}{dt}&=\left(-\frac{2}{\tau_{ext}}-\frac{1}{\tau_0}-O^{\ P}_{g\,l,m,n}+i\Delta\omega\right)A^{P}_{l,m,n}-i\sqrt{\frac{2}{\tau_{ext}\tau}}A^{P}_{in.l,m,n}\\ \frac{dA^{S}_{l,m,n}}{dt}&=\left(-\frac{2}{\tau_{ext}}-\frac{1}{\tau_0}-O^{\ S}_{g\,l,m,n}+i\Delta\omega\right)A^{S}_{l,m,n}\\ &+\frac{c}{2n_{eff}}\sum_q N_i^q\sigma_{ji}\left(\omega_{WGM}\right)\Omega^{q,S}_{l,m,n}A_0-i\sqrt{\frac{2}{\tau_{ext}\tau}}A^{S}_{in.l,m,n}\end{aligned}\tag{11}$$

with

$$O^{\ y}_{g\,l,m,n}=\frac{c}{2n_{eff}}\left(\sum_q N_i^q\sigma_{ji}\left(\omega_{WGM}\right)\Omega^{q,y}_{l,m,n}-\sum_q N_i^q\sigma_{ij}\left(\omega_{WGM}\right)\Omega^{q,y}_{l,m,n}\right).\tag{12}$$

with $y = P, S$.

The gain g of the amplifier is:

$$g=\left|\frac{A^{y}_{out,l,m,n}}{A^{y}_{in,l,m,n}}\right|^2\tag{13}$$

where $A^{y}_{in,l,m,n}$ is the input and $A^{y}_{out,l,m,n}$ the output slowly varying amplitudes which scale the normalized electric field on the $r-\theta$ plane; $\tau=2\pi\rho_0 n_{eff}/c$ is the circulation time inside the microsphere, ρ_0 is the microsphere radius, n_{eff} is the WGM effective refractive index, c the speed of light in vacuum; $\Delta\omega=\omega_{in}-\omega_{WGM}$ is the frequency detuning of the fiber input signal from the WGM resonance frequency; $\tau_0=1/\kappa_0^2=Q_0/\omega_{WGM}$, Q_0 is the intrinsic quality factor and κ_0 is the intrinsic cavity decay rate; $\tau_{ext}=m\pi/\left(\omega\kappa^2\right)$ is the coupling lifetime; κ is the cavity decay rate or coupling coefficient, calculated via the overlap integral between the electromagnetic field of the fiber guided mode and the microsphere WGMs [13]; ω_{WGM} is the WGMs resonant frequency; $\sigma_{ij}\left(\omega_{WGM}\right)$ is the erbium cross-section at frequency ω_{WGM}; $\Omega^{q,y}_{l,m,n}$ with y = P, S is the overlap factor of each WGM with the rare earth profile in the q-th sector expressed in Eq. (14):

$$\Omega^{q,y}_{l,m,n}=\iint_{A_q}\left|K^{y}_{l,m,n}\left(r,\theta\right)\right|^2 r dr d\theta,\tag{14}$$

where $K^{y}_{l,m,n}\left(r,\theta\right)$ is the normalized electric field on the plane $\hat{r}\cdot\hat{\theta}$ and A_q is the area of q-th sector.

Funding

This research was performed within MIUR plans: PON01 01224 “Sviluppo di tecnologie in guida d’onda integrata (SIW) per applicazioni ICT a microonde”; PONa3 00298 “Potenziamento delle strutture e delle dotazioni scientifiche e tecnologiche del polo scientifico e tecnologico Magna Grecia”; PON02 00576 3329762 “Sistemi avanzati mini-invasivi di diagnosi e radioterapia” AMIDERHA; COST Action MP1401 Advanced Fibre Laser and Coherent Source as tools for Society, Manufacturing and Lifescience.